

Narrow Tilting Vehicle Drifting Robust Control

Dongxin Xu ^{1,*} , Yueqiang Han ¹ , Xianghui Han ¹, Ya Wang ² and Guoye Wang ^{1,*}¹ College of Engineering, China Agricultural University, Beijing 100083, China² Beijing Zuoqi Technology Ltd., Beijing 101300, China* Correspondence: xudongxin1996@163.com (D.X.); wgy1615@126.com (G.W.);
Tel.: +86-010-6273-6856 (D.X.); +86-182-1093-7906 (G.W.)

Abstract: The narrow tilting vehicle receives extensive public attention because of traffic congestion and environmental pollution, and the active rolling motion control is a traffic safety precaution that reduces the rollover risk caused by the structure size of the narrow vehicle. The drifting motion control reflects the relatively updated attentive research of the regular-size vehicle, which can take full advantage of the vehicle's dynamic performance and improve driving safety, especially when tires reach their limits. The narrow tilting vehicle drifting control is worthy of research to improve the driving safety of the narrow tilting vehicle, especially when tires reach the limit. The nonlinear narrow tilting vehicle dynamic model is established with the UniTire model to describe the vehicle motion characteristics and is simplified to reduce the computation of the drifting controller design. The narrow tilting vehicle drifting controller is designed based on the robust theory with uncertain external disturbances. The controller has a wide application, validity, and robustness and whose performance is verified by realizing different drifting motions with different initial driving motions. The narrow tilting vehicle drifting robust control has some practical and theoretical significance for more research.

Keywords: narrow tilting vehicle; drifting motion; robust controller



Citation: Xu, D.; Han, Y.; Han, X.; Wang, Y.; Wang, G. Narrow Tilting Vehicle Drifting Robust Control. *Machines* **2023**, *11*, 90. <https://doi.org/10.3390/machines11010090>

Academic Editor: Jian Wu

Received: 12 December 2022

Revised: 8 January 2023

Accepted: 9 January 2023

Published: 10 January 2023



Copyright: © 2023 by the authors. Licensee MDPI, Basel, Switzerland. This article is an open access article distributed under the terms and conditions of the Creative Commons Attribution (CC BY) license (<https://creativecommons.org/licenses/by/4.0/>).

1. Introduction

With increasing population and rapid economic development, there are continuing high numbers of vehicle population as [1] and traffic accidents as [2,3]. The mini-size vehicle has been paid close attention to universally, and the narrow tilting vehicle entered the public consciousness. The narrow tilting vehicle is designed to solve traffic congestion and environmental pollution problems caused by the vehicle's rapid growth. Furthermore, the active rolling motion of the narrow tilting vehicle is the steady state realized by the active rolling controller based on the velocity and the steering angle to avoid the rollover.

Traffic safety is in constant focus [4], and most relative research includes the autonomous steering of the regular-size vehicle [5] and the active rolling of the narrow vehicle. The autonomous steering of regular-size vehicle research is almost wholly working under the linear vehicle and tire condition, such as the path following in [6] and the human-machine cooperation driving in [7]. Most traffic safety research on narrow vehicles has looked at how to reduce the rollover risk. The active rolling of the narrow vehicle can improve turning driving safety and avoid the rollover risk caused by the narrow size. The narrow vehicle is divided into direct tilt control and steering tilt control [8] based on active rolling methods. It is also divided into the four-wheel [9], the three-wheel [10], and the reversed three-wheel [11] based on the structures. The direct tilt control of the narrow tilting vehicle is directly applied to the vehicle body, but it has poor adaptability under different working conditions. The narrow tilting vehicle based on the steering tilting control realizes the active rolling based on the steering angle, but it needs the driving technique and is not well suited at the low longitudinal velocity. The narrow tilting vehicle studied in this paper is a four-wheel narrow tilting vehicle with direct tilt control based on the steering

angle [12] to improve driving safety at a multi-level velocity in different steering angles. The active rolling target angle is the steady state calculated based on the centrifugal force balance analysis in [13], which is realized by relying on the active rolling mechanic [12,14]. The narrow tilting vehicle studied in this paper is verified whereby the active rolling angle can realize the steady-state target and lower the rollover risk significantly by the active rolling mechanic and controller [12–14]. Most other traffic safety research on the narrow tilting vehicle focuses on vehicle performance under normal working conditions, as seen in one study [15].

The drifting motion control is a unique control strategy available to enhance traffic safety, which is little used in narrow drifting motions. The drifting movement of the racing car can be controlled by the drifting controller, which realizes the target drifting motion analyzed based on the three-of-freedom vehicle dynamics model when tires reach the maximum in [16]. The regular-size vehicle drifting motion parameters, including velocity, sideslip angle, yaw rate, and steering angle can be calculated and obtained by analyzing the steady-state vehicle dynamics expressions in the adhesion limit [17], and the drifting controllers of a regular-size vehicle are designed based on the linear quadratic regulator theory [17–19], the model predictive control theory [20,21], and the adaptive control theory [22]. There is reinforcement learning [18], and neural networks [23] are applied to the vehicle drifting control based on existing vehicle drifting motion parameters. Most drifting research without the learning realize the target drifting motion, which is the core work, and ignores some important details which affect the practical implementation, especially disturbances. Most drifting research based on the learning realize the passed path under drifting motions, and the adaptability in different working conditions are not fully verified, and most vehicle dynamics models of drifting movements are very similar to the classic one [24] that suggests vehicle dynamics with no-active rolling. According to the narrow tilting vehicle characteristics, it is necessary to design a drifting controller with extensive suitability with external disturbances to improve driving safety when tires reach the maximum. The robust theory performs better in solving problems caused by disturbances and can accommodate engineering requirements in practice. The linear matrix inequality (LMI) is widely applied in solving the problems of controller and system designs, which has become popular in the controller solution, especially in the robust controller.

From the above analysis, this paper researches how to control the narrow tilting vehicle drifting motions. According to the narrow tilting vehicle characteristics, the non-linear narrow tilting vehicle dynamics model is established to describe the vehicle motion characteristics and is appropriately simplified to reduce the computing effort in the drifting controller design. The narrow tilting vehicle drifting controller is designed based on the robust theory with uncertain external disturbances considering the practical application environment, which is relatively independent and does not affect the active rolling controller working. The performance of the drifting controller is tested to realize different target drifting motions based on different initial motions, which can express the reliability, availability, and universality of the designed controller.

2. Narrow Tilting Vehicle Dynamics System for Drifting Controller Design

The narrow tilting vehicle shown in Figure 1a, whose structural diagram is shown in Figure 1b in [25], avoids rollover danger by the active roll control, which is different from most vehicles. To ensure all wheels are on the ground and avoid rollover, the rolling controller of the narrow tilting vehicle creates a good balance between the gravity component caused by rolling and centrifugal force caused by turning [12–14].

The vehicle dynamics system is requested to describe the narrow tilting vehicle drifting motion characteristics and is applied to the controller design to realize target motions. The rolling motion of the narrow tilting vehicle is different from most vehicles; as a result, the major influence factors of the vertical load transfer are distinctive. The drifting motion is a unique motion state for the vehicle, and tire forces reach limits in the drifting motion. Therefore, the tire model also has an essential effect on the controller design.

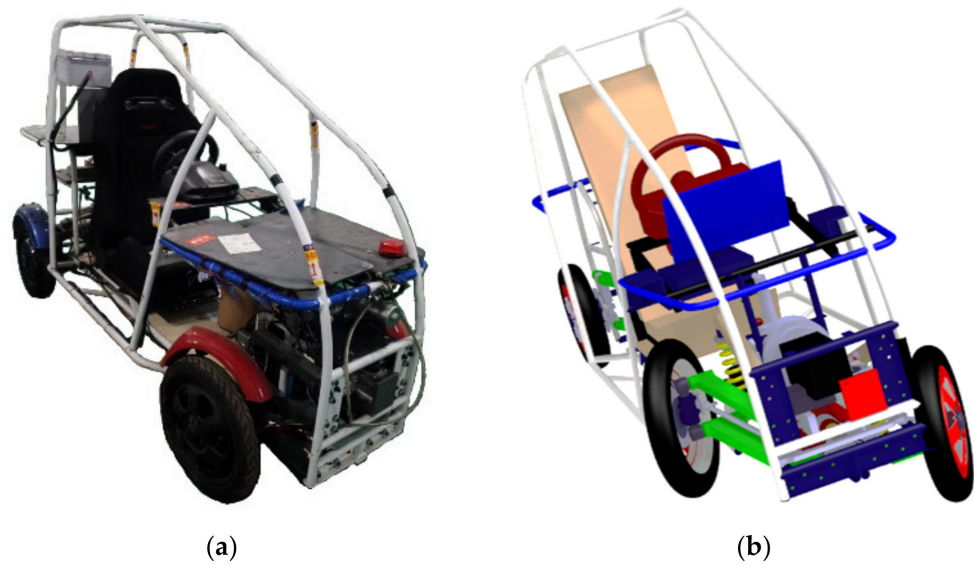


Figure 1. The narrow tilting vehicle: (a) the physical; (b) the structural [25].

2.1. Narrow Tilting Vehicle Dynamics Equations

The active rolling movement meets the need for the active rolling angle for the centrifugal force equilibrium based on narrow tilting vehicle dynamics characteristics. The vehicle dynamics model, including the active rolling movement, is shown in Figure 2 and is described as Equations (1)–(4), where Equation (5) describes the normal rolling motion without the active rolling mechanic.

$$\dot{v} = (F_{xfl} + F_{xfr}) \left(\frac{\cos \delta_f \cos \beta}{m} + \frac{\sin \delta_f \sin \beta}{m} \right) + (F_{yfl} + F_{yfr}) \left(-\frac{\sin \delta_f \cos \beta}{m} + \frac{\cos \delta_f \sin \beta}{m} \right) + (F_{xrl} + F_{xrr}) \frac{\cos \beta}{m} + (F_{yrl} + F_{yrr}) \frac{\sin \beta}{m} - \frac{C_d A_f v^2 \cos^3 \beta}{21.15m}, \quad (1)$$

$$\dot{\beta} = -\gamma + (F_{xfl} + F_{xfr}) \left(\frac{\sin \delta_f \cos \beta}{mv} - \frac{\cos \delta_f \sin \beta}{mv} \right) + (F_{yfl} + F_{yfr}) \left(\frac{\cos \delta_f \cos \beta}{mv} + \frac{\sin \delta_f \sin \beta}{mv} \right) - (F_{xrl} + F_{xrr}) \frac{\sin \beta}{mv} + (F_{yrl} + F_{yrr}) \frac{\cos \beta}{mv} + \frac{C_d A_f v \cos^2 \beta \sin \beta}{21.15m}, \quad (2)$$

$$\dot{\gamma} = \frac{l_f}{I_z} (F_{xfl} + F_{xfr}) \sin \delta_f + \frac{l_f}{I_z} (F_{yfl} + F_{yfr}) \cos \delta_f - \frac{l_r}{I_z} (F_{yrl} + F_{yrr}) - \frac{w_f}{2I_z} (F_{xfl} - F_{xfr}) \cos \delta_f + \frac{w_f}{2I_z} (F_{yfl} - F_{yfr}) \sin \delta_f - \frac{w_r}{2I_z} (F_{xrl} - F_{xrr}), \quad (3)$$

$$\psi = -\tan^{-1} \frac{v^2}{gR_r}, \quad (4)$$

$$\ddot{\psi} = \frac{I_{xz}}{I_x} \dot{\gamma} + \frac{m_b h_b}{I_x} (\dot{v}_y + v_x \gamma) + \frac{m_b g h_b}{I_x} \sin \psi - \frac{K_\psi \psi + C_\psi \dot{\psi}}{I_x} \quad (5)$$

where m is the vehicle mass, m_b is the vehicle body mass, h_b is the height of gravity center from the roll axis, l_f and l_r are the distances from gravity center to front and rear axle, w_f and w_r are the distances between left and right wheels of the front and rear axle, $R_r = (l_f + l_r) / \delta_f$ is the ideal turning radius calculated based on the steering angle, v and \dot{v} are the vehicle velocity and accelerated velocity, β and $\dot{\beta}$ are the vehicle sideslip angle and rate, γ and $\dot{\gamma}$ are the vehicle yaw rate and angular acceleration, δ_f is the front-wheel steering angle, ψ is the vehicle steady roll angle and is implemented by the active roll controller, I_z is the moment of inertia with respect to yaw axis, C_d is the aerodynamics drag coefficient, A_f is the vehicle frontal area, and F_{xij} and F_{yij} ($i = f, r$; $j = l, r$) are the longitudinal and lateral forces at each tire, respectively, the index $i = f, r$ is used to express the front and rear axles, and the index $j = l, r$ is used to express the left and right wheels.

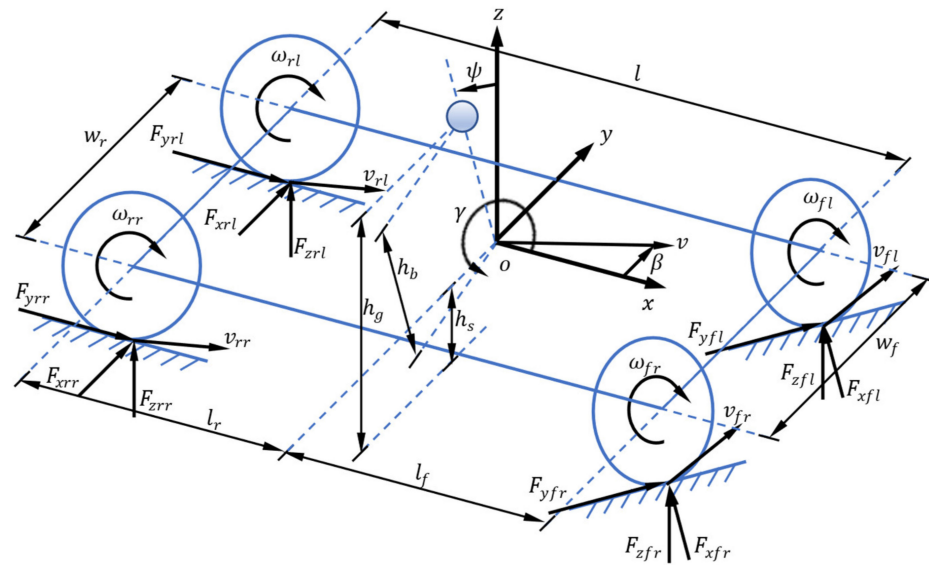


Figure 2. The vehicle dynamics model.

2.2. Vertical Load Transfer

The rolling movement of the narrow tilting vehicle is distinctive. The roll angle has a significant influence on the vertical load transfer. Considering the load transfer caused by longitudinal and lateral forces and the active roll control shown in Figure 3, the vertical force at each tire can be described as Equations (6)–(9).

$$F_{zfl} = \frac{mgl_r}{2(l_f + l_r)} - \frac{F_{sx}h_g}{2(l_f + l_r)} - \frac{l_r(F_{sy}h_g \cos \psi + m_bgh_b \sin \psi)}{(l_f + l_r)w_f}, \tag{6}$$

$$F_{zfr} = \frac{mgl_r}{2(l_f + l_r)} - \frac{F_{sx}h_g}{2(l_f + l_r)} + \frac{l_r(F_{sy}h_g \cos \psi + m_bgh_b \sin \psi)}{(l_f + l_r)w_f}, \tag{7}$$

$$F_{zrl} = \frac{mgl_f}{2(l_f + l_r)} + \frac{F_{sx}h_g}{2(l_f + l_r)} - \frac{l_f(F_{sy}h_g \cos \psi + m_bgh_b \sin \psi)}{(l_f + l_r)w_r}, \tag{8}$$

$$F_{zrr} = \frac{mgl_f}{2(l_f + l_r)} + \frac{F_{sx}h_g}{2(l_f + l_r)} + \frac{l_f(F_{sy}h_g \cos \psi + m_bgh_b \sin \psi)}{(l_f + l_r)w_r}, \tag{9}$$

where h_g is the height of gravity center, $F_{sx} = (F_{xfl} + F_{xfr}) \cos \delta_f - (F_{yfl} + F_{yfr}) \sin \delta_{fl} + (F_{xrl} + F_{xrr}) - C_d A_f v^2 \cos^3 \beta / (21.15m)$, and $F_{sy} = (F_{xfl} + F_{xfr}) \sin \delta_{fl} + (F_{yfl} + F_{yfr}) \cos \delta_{fl} + (F_{yrl} + F_{yrr})$.

2.3. Tire Models and Equations

The vehicle drifting motion is nonlinear, and tire forces reach the maximum while the steering angle is non-vanishing in the drifting motion. Therefore, the nonlinear tire model is essential in this system to describe the force condition at each tire. The UniTire tire model can express tire forces more accurately not only in single working conditions but also in complex working conditions [26], which means it is ideally suited to the part of the vehicle drifting motion. If the UniTire tire model is applied directly to the narrow tilting vehicle drifting controller, there will be a large amount of computation in the controller design. The linearized tire model based on UniTire is proposed in the controller design to solve this problem and express tire forces accurately. Thus, UniTire describes tire forces during the narrow tilting vehicle motion, and the linearized tire model is applied to the narrow tilting drifting controller design.

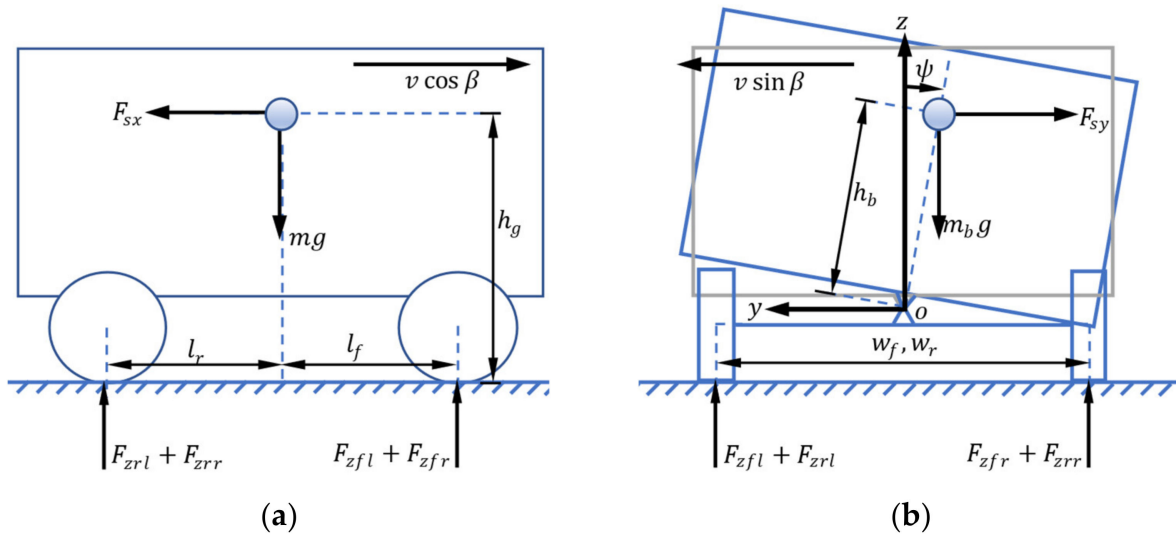


Figure 3. The vertical load transfer: (a) the longitudinal movement caused; (b) the lateral and active roll movements caused.

2.3.1. UniTire

UniTire can express longitudinal and lateral tire forces and overturning, rolling resistance, and aligning tire moments based on the tire coordinate system and is applied to the vehicle dynamics simulation and the vehicle motion controller design [27]. In this paper, the tire model is applied to express longitudinal and lateral tire forces, which are the main characteristics of different working conditions. Thus, the simplified tire coordinate system is shown in Figure 4 with the consideration of longitudinal and lateral tire motions and the neglect of tire moments, and the equations of the tire model are described as Equation (10).

$$\begin{cases} \bar{F}_{ij} = 1 - e^{-\phi_{ij} - E\phi_{ij}^2 - (E^2 + \frac{1}{12})\phi_{ij}^3} \\ F_{xij} = \bar{F}_{ij} \frac{\phi_{xij}}{\phi_{ij}} \mu_{xij} F_{zij} \\ F_{yij} = \bar{F}_{ij} \frac{\phi_{yij}}{\phi_{ij}} \mu_{yij} F_{zij} \end{cases}, \quad (10)$$

where \bar{F}_{ij} ($i = f, r; j = l, r$) is the normalized force, E is the curvature factor of the combined slip resultant force and is the variable related to the tire slip ratios in [28], μ_{xij} and μ_{yij} ($i = f, r; j = l, r$) are the longitudinal and lateral friction coefficient, $\phi_{xij} = K_{xij} S_{xij} / (\mu_{xij} F_{zij})$, $\phi_{yij} = K_{yij} S_{yij} / (\mu_{yij} F_{zij})$, and $\phi_{ij} = \sqrt{\phi_{xij}^2 + \phi_{yij}^2}$ ($i = f, r; j = l, r$) are normalized longitudinal, lateral and combined slip ratios, $S_{xij} = (\omega_{ij} r_{eij} - v_{ij} \cos \alpha_{ij}) / (\omega_{ij} r_{eij})$ and $S_{yij} = -v_{ij} \sin \alpha_{ij} / (\omega_{ij} r_{eij})$ ($i = f, r; j = l, r$) are the longitudinal and lateral slip ratios in UniTire, K_{xij} and K_{yij} ($i = f, r; j = l, r$) are the longitudinal slip and cornering stiffness of the tire based on S_{xij} and S_{yij} , v_{ij} ($i = f, r; j = l, r$) is the wheel velocity, ω_{ij} ($i = f, r; j = l, r$) is the wheel rotation angular velocity, r_{eij} ($i = f, r; j = l, r$) is the wheel effective rolling radius, α_{ij} ($i = f, r; j = l, r$) is the wheel slip angle, and the wheel slip angle of each wheel respectively satisfy $\alpha_{fl} = \tan^{-1}((-a_{fl} \sin \delta_f + (v \sin \beta + l_f \gamma) \cos \delta_f) / (a_{fl} \cos \delta_f + (v \sin \beta + l_f \gamma) \sin \delta_f))$, $\alpha_{fr} = \tan^{-1}((-a_{fr} \sin \delta_f + (v \sin \beta + l_f \gamma) \cos \delta_f) / (a_{fr} \cos \delta_f + (v \sin \beta + l_f \gamma) \sin \delta_f))$, $\alpha_{rl} = \tan^{-1}((v \sin \beta - l_r \gamma) / (v \cos \beta - w_r \gamma / 2))$, and $\alpha_{rr} = \tan^{-1}((v \sin \beta - l_r \gamma) / (v \cos \beta + w_r \gamma / 2))$ in which $a_l = v \cos \beta - w_f \gamma / 2$ and $a_r = v \cos \beta + w_f \gamma / 2$.

2.3.2. The Linearized Tire Equations

UniTire is a nonlinear tire model, and its tire force equations are complicated for the controller design. The linearized tire equations are derived based on the representation of the nonlinear tire model. The TYDEX longitudinal slip ratio is the common expression, and the nonlinear tire model representation is shown in Figure 5.

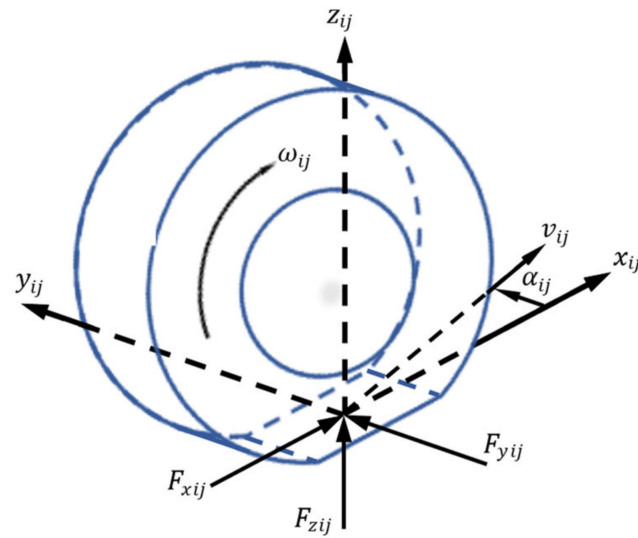


Figure 4. Simplified tire coordinate system.

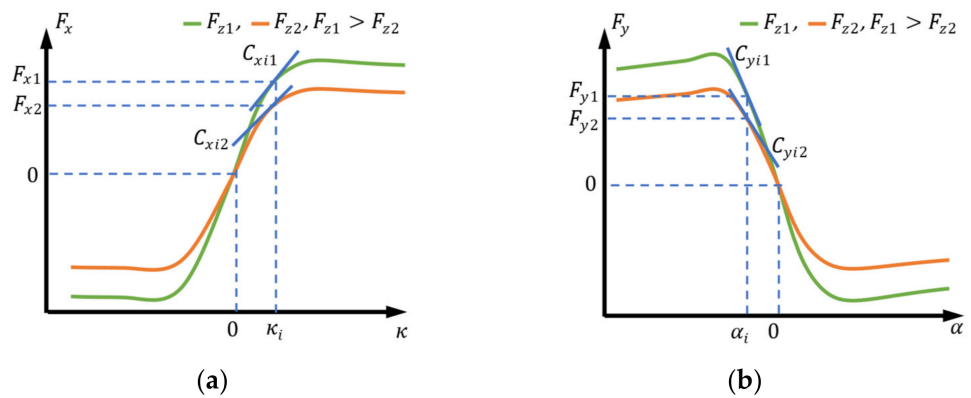


Figure 5. The representation of UniTire: (a) the longitudinal tire force in which κ_i is the TYDEX longitudinal slip ratio and C_{xi1} and C_{xi2} are slip stiffnesses under different vertical forces F_{z1} and F_{z2} ; (b) the lateral tire force in which C_{yi1} and C_{yi2} cornering stiffnesses under different vertical forces F_{z1} and F_{z2} .

According to the UniTire representation, the nonlinear tire model can be approximately linearized and divided into many groups. The slip angles of the left and right wheels in the same axle are less differentiating based on the expression of slip angles, which has a slight influence on tire forces, and it suggests that the value of the vertical force makes a difference to the tire force value, the slip stiffness, and the cornering stiffness in Figure 5. The linearized tire equations are described as Equation (11) with the consideration of the simplified calculation of the controller system and the independent control of the front and rear axles.

$$\begin{cases} F_{xij} = \hat{C}_{xij}(\kappa_i - \hat{\kappa}_i) + \hat{F}_{xij} \\ F_{yij} = \hat{C}_{yij}(\alpha_i - \hat{\alpha}_i) + \hat{F}_{yij} \end{cases} \quad (11)$$

where $\kappa_i = -(v_i \cos \alpha_i - \omega_i r_{ei}) / (v_i \cos \alpha_i)$ ($i = f, r$) is the TYDEX longitudinal slip ratio, $\hat{\kappa}_i$, $\hat{\alpha}_i$, \hat{C}_{xij} , \hat{C}_{yij} , \hat{F}_{xij} , and \hat{F}_{yij} are the known slip ratio, slip angle, slip stiffness, cornering stiffness, longitudinal force, and lateral force of the approximation point, respectively, $\alpha_f = \tan^{-1}((-v \cos \beta \sin \delta_f + (v \sin \beta + l_f \gamma) \cos \delta_f) / (v \cos \beta \cos \delta_f + (v \sin \beta + l_f \gamma) \sin \delta_f))$ is the slip angle of the front axle, and $\alpha_r = \tan^{-1}((v \sin \beta - l_r \gamma) / (v \cos \beta))$ is the slip angle of the rear axle.

3. Narrow Tilting Vehicle Drifting Controller Design

A block scheme of the narrow tilting vehicle drifting control strategy is shown as Figure 6. Considering uncertain external disturbances, d_e , the narrow tilting vehicle drifting controller is designed based on robust theory to realize the target drifting motion, including the target velocity v_{target} , the target sideslip angle β_{target} , the target yaw rate γ_{target} , the target steering angle δ_{f_target} , the target longitudinal slip ratio of the front axle κ_{f_target} , and the target longitudinal slip ratio of the rear axle, κ_{r_target} .

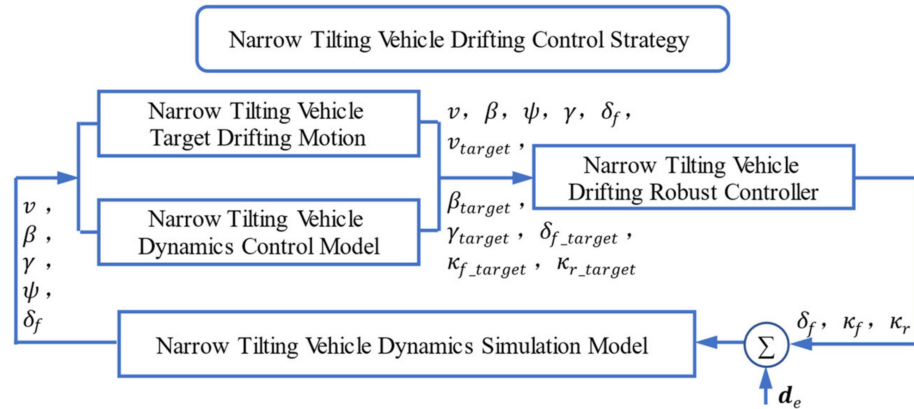


Figure 6. Narrow tilting vehicle drifting control strategy.

3.1. Controller System State-Space Expression

According to the above, the narrow tilting vehicle can be described as Equation (12).

$$\begin{bmatrix} \dot{v} \\ \dot{\beta} \\ \dot{\gamma} \\ \dot{\Psi} \end{bmatrix} = \begin{bmatrix} \frac{\partial \dot{v}}{\partial v} & \frac{\partial \dot{v}}{\partial \beta} & \frac{\partial \dot{v}}{\partial \gamma} & 0 \\ \frac{\partial \dot{\beta}}{\partial v} & \frac{\partial \dot{\beta}}{\partial \beta} & \frac{\partial \dot{\beta}}{\partial \gamma} & 0 \\ \frac{\partial \dot{\gamma}}{\partial v} & \frac{\partial \dot{\gamma}}{\partial \beta} & \frac{\partial \dot{\gamma}}{\partial \gamma} & 0 \\ \frac{\partial \dot{\Psi}}{\partial v} & 0 & 0 & 0 \end{bmatrix} \begin{bmatrix} v \\ \beta \\ \gamma \\ \Psi \end{bmatrix} + \begin{bmatrix} \frac{\partial \dot{v}}{\partial \delta_f} & \frac{\partial \dot{v}}{\partial \kappa_f} & \frac{\partial \dot{v}}{\partial \kappa_r} \\ \frac{\partial \dot{\beta}}{\partial \delta_f} & \frac{\partial \dot{\beta}}{\partial \kappa_f} & \frac{\partial \dot{\beta}}{\partial \kappa_r} \\ \frac{\partial \dot{\gamma}}{\partial \delta_f} & \frac{\partial \dot{\gamma}}{\partial \kappa_f} & \frac{\partial \dot{\gamma}}{\partial \kappa_r} \\ \frac{\partial \dot{\Psi}}{\partial \delta_f} & 0 & 0 \end{bmatrix} \begin{bmatrix} \delta_f \\ \kappa_f \\ \kappa_r \end{bmatrix}, \quad (12)$$

where Ψ is the integral value of the rolling angle ψ , and

$$\frac{\partial \dot{v}}{\partial v} = -\frac{2C_d A_f v \cos^3 \beta}{21.15m} + \frac{\hat{C}_{yfl} + \hat{C}_{yfr}}{m} \left(-\sin \delta_f \cos \beta + \cos \delta_f \sin \beta \right) \times \frac{\partial \alpha_f}{\partial v} + \frac{(\hat{C}_{yrl} - \hat{C}_{yrr}) \sin \beta}{m} \times \frac{\partial \alpha_r}{\partial v},$$

$$\begin{aligned} \frac{\partial \dot{v}}{\partial \beta} &= \frac{3C_d A_f v^2 \cos^2 \beta \sin \beta}{21.15m} + \left(\frac{F_{xfl} + F_{xfr}}{m} - \frac{\hat{C}_{yfl} + \hat{C}_{yfr}}{m} \times \frac{\partial \alpha_f}{\partial \beta} \right) \left(-\cos \delta_f \sin \beta + \sin \delta_f \cos \beta \right) \\ &+ \frac{F_{yfl} + F_{yfr}}{m} \left(\sin \delta_f \sin \beta + \cos \delta_f \cos \beta \right) - \left(\frac{F_{xrl} + F_{xrr}}{m} - \frac{\hat{C}_{yrl} + \hat{C}_{yrr}}{m} \times \frac{\partial \alpha_r}{\partial \beta} \right) \sin \beta + \frac{(F_{yrl} + F_{yrr}) \cos \beta}{m}, \end{aligned}$$

$$\begin{aligned} \frac{\partial \dot{v}}{\partial \beta} &= \frac{3C_d A_f v^2 \cos^2 \beta \sin \beta}{21.15m} + \left(\frac{F_{xfl} + F_{xfr}}{m} - \frac{\hat{C}_{yfl} + \hat{C}_{yfr}}{m} \times \frac{\partial \alpha_f}{\partial \beta} \right) \left(-\cos \delta_f \sin \beta + \sin \delta_f \cos \beta \right) \\ &+ \frac{F_{yfl} + F_{yfr}}{m} \left(\sin \delta_f \sin \beta + \cos \delta_f \cos \beta \right) - \left(\frac{F_{xrl} + F_{xrr}}{m} - \frac{\hat{C}_{yrl} + \hat{C}_{yrr}}{m} \times \frac{\partial \alpha_r}{\partial \beta} \right) \sin \beta + \frac{(F_{yrl} + F_{yrr}) \cos \beta}{m}, \end{aligned}$$

$$\frac{\partial \dot{v}}{\partial \gamma} = \frac{\hat{C}_{yfl} + \hat{C}_{yfr}}{m} \left(-\sin \delta_f \cos \beta + \cos \delta_f \sin \beta \right) \times \frac{\partial \alpha_f}{\partial \gamma} + \frac{(\hat{C}_{yrl} + \hat{C}_{yrr}) \sin \beta}{m} \times \frac{\partial \alpha_r}{\partial \gamma},$$

$$\frac{\partial \dot{v}}{\partial \delta_f} = \left(\frac{F_{xfl} + F_{xfr}}{m} + \frac{\hat{C}_{yfl} + \hat{C}_{yfr}}{m} \times \frac{\partial \alpha_f}{\partial \delta_f} \right) \left(-\sin \delta_f \cos \beta + \cos \delta_f \sin \beta \right) - \frac{F_{yfl} + F_{yfr}}{m} \left(\cos \delta_f \cos \beta + \sin \delta_f \sin \beta \right),$$

$$\frac{\partial \dot{v}}{\partial \kappa_f} = \frac{(\hat{C}_{xfl} + \hat{C}_{xfr}) (\cos \delta_f \cos \beta + \sin \delta_f \sin \beta)}{m},$$

$$\begin{aligned} \frac{\partial \dot{\beta}}{\partial v} &= \frac{C_d A_f \cos^2 \beta \sin \beta}{21.15m} + \frac{F_{xfl} + F_{xfr}}{mv^2} (-\sin \delta_f \cos \beta + \cos \delta_f \sin \beta) + \frac{F_{yfl} + F_{yfr}}{mv^2} (-\cos \delta_f \cos \beta - \sin \delta_f \sin \beta) \\ &+ \frac{\hat{C}_{yfl} + \hat{C}_{yfr}}{mv} (\cos \delta_f \cos \beta + \sin \delta_f \sin \beta) \times \frac{\partial \alpha_f}{\partial v} + \frac{(\hat{C}_{yrl} + \hat{C}_{yrr}) \cos \beta}{mv} \times \frac{\partial \alpha_r}{\partial v} + \frac{(F_{xrl} + F_{xrr}) \sin \beta}{mv^2} - \frac{(F_{yrl} + F_{yrr}) \cos \beta}{mv^2}, \\ \frac{\partial \dot{\beta}}{\partial \beta} &= \frac{C_d A_f v \cos^3 \beta}{21.15m} - \frac{2C_d A_f v \sin^2 \beta \cos \beta}{21.15m} - \left(\frac{F_{xfl} + F_{xfr}}{mv} - \frac{\hat{C}_{yfl} + \hat{C}_{yfr}}{mv} \times \frac{\partial \alpha_f}{\partial \beta} \right) (\sin \delta_f \sin \beta + \cos \delta_f \cos \beta) \\ &+ \frac{F_{yfl} + F_{yfr}}{mv} (-\cos \delta_f \sin \beta + \sin \delta_f \cos \beta) - \left(\frac{F_{xrl} + F_{xrr}}{mv} - \frac{\hat{C}_{yrl} + \hat{C}_{yrr}}{mv} \times \frac{\partial \alpha_r}{\partial \beta} \right) \cos \beta - \frac{(F_{yrl} + F_{yrr}) \sin \beta}{mv}, \\ \frac{\partial \dot{\beta}}{\partial \gamma} &= -1 + \frac{\hat{C}_{yfl} + \hat{C}_{yfr}}{mv} (\cos \delta_f \cos \beta + \sin \delta_f \sin \beta) \times \frac{\partial \alpha_f}{\partial \gamma} + \frac{(\hat{C}_{yrl} + \hat{C}_{yrr}) \cos \beta}{mv} \times \frac{\partial \alpha_r}{\partial \gamma}, \\ \frac{\partial \dot{\beta}}{\partial \delta_f} &= \left(\frac{F_{xf}}{mv} + \frac{\hat{C}_{yfl} + \hat{C}_{yfr}}{mv} \times \frac{\partial \alpha_f}{\partial \delta_f} \right) (\cos \delta_f \cos \beta + \sin \delta_f \sin \beta) + \frac{F_{yfl}}{mv} (-\sin \delta_f \cos \beta + \cos \delta_f \sin \beta), \\ \frac{\partial \dot{\beta}}{\partial \kappa_f} &= \frac{\hat{C}_{xfl} + \hat{C}_{xfr}}{mv} (\sin \delta_f \cos \beta - \cos \delta_f \sin \beta), \quad \frac{\partial \dot{\beta}}{\partial \kappa_r} = -\frac{(\hat{C}_{xrl} + \hat{C}_{xrr}) \sin \beta}{mv}, \\ \frac{\partial \dot{\gamma}}{\partial v} &= \frac{l_f (\hat{C}_{yfl} + \hat{C}_{yfr})}{I_z} \cos \delta_f \times \frac{\partial \alpha_f}{\partial v} - \frac{l_r (\hat{C}_{yrl} + \hat{C}_{yrr})}{I_z} \times \frac{\partial \alpha_r}{\partial v} + \frac{w_f (\hat{C}_{yfl} - \hat{C}_{yfr})}{2I_z} \sin \delta_f \times \frac{\partial \alpha_f}{\partial v}, \\ \frac{\partial \dot{\gamma}}{\partial \beta} &= \frac{l_f (\hat{C}_{yfl} + \hat{C}_{yfr})}{I_z} \cos \delta_f \times \frac{\partial \alpha_f}{\partial \beta} - \frac{l_r (\hat{C}_{yrl} + \hat{C}_{yrr})}{I_z} \times \frac{\partial \alpha_r}{\partial \beta} + \frac{w_f (\hat{C}_{yfl} - \hat{C}_{yfr})}{2I_z} \sin \delta_f \times \frac{\partial \alpha_f}{\partial \beta}, \\ \frac{\partial \dot{\gamma}}{\partial \gamma} &= \frac{l_f (\hat{C}_{yfl} + \hat{C}_{yfr})}{I_z} \cos \delta_f \times \frac{\partial \alpha_f}{\partial \gamma} - \frac{l_r (\hat{C}_{yrl} + \hat{C}_{yrr})}{I_z} \times \frac{\partial \alpha_r}{\partial \gamma} + \frac{w_f (\hat{C}_{yfl} - \hat{C}_{yfr})}{2I_z} \sin \delta_f \times \frac{\partial \alpha_f}{\partial \gamma}, \\ \frac{\partial \dot{\gamma}}{\partial \delta_f} &= \frac{l_f \cos \delta_f}{I_z} (F_{xf} + (\hat{C}_{yfl} + \hat{C}_{yfr}) \times \frac{\partial \alpha_f}{\partial \delta_f}) + \frac{w_f \cos \delta_f}{2I_z} ((\hat{C}_{yfl} - \hat{C}_{yfr}) (\alpha_f - \hat{\alpha}_f) + (\hat{F}_{yfl} - \hat{F}_{yfr})) \\ &+ \frac{w_f \sin \delta_f}{2I_z} ((\hat{C}_{xfl} - \hat{C}_{xfr}) (\kappa_f - \hat{\kappa}_f) + (\hat{F}_{xfl} - \hat{F}_{xfr})) + (\hat{C}_{yfl} - \hat{C}_{yfr}) \times \frac{\partial \alpha_f}{\partial \delta_f} - \frac{F_{yfl} l_f}{I_z} \sin \delta_f, \\ \frac{\partial \dot{\gamma}}{\partial \kappa_f} &= \frac{l_f (\hat{C}_{xfl} + \hat{C}_{xfr})}{I_z} \sin \delta_f - \frac{w_f (\hat{C}_{xfl} - \hat{C}_{xfr})}{2I_z} \cos \delta_f, \quad \frac{\partial \dot{\gamma}}{\partial \kappa_r} = -\frac{w_r (\hat{C}_{xrl} - \hat{C}_{xrr})}{2I_z}, \\ \frac{\partial \psi}{\partial v} &= -\frac{2v \delta_f g (l_f + l_r)}{g^2 (l_f + l_r)^2 + v^4 \delta_f^2}, \quad \frac{\partial \psi}{\partial \delta_f} = \frac{v^2 g (l_f + l_r)}{g^2 (l_f + l_r)^2 + v^4 \delta_f^2} \end{aligned}$$

in which

$$\begin{aligned} \frac{\partial \alpha_f}{\partial v} &= -\frac{\gamma l_f \cos \beta}{v^2 + 2v \gamma l_f \sin \beta + \gamma^2 l_f^2}, \quad \frac{\partial \alpha_f}{\partial \beta} = \frac{v^2 + v \gamma l_f \sin \beta}{v^2 + 2v \gamma l_f \sin \beta + \gamma^2 l_f^2}, \\ \frac{\partial \alpha_f}{\partial \gamma} &= \frac{v l_f \cos \beta}{v^2 + 2v \gamma l_f \sin \beta + \gamma^2 l_f^2}, \quad \frac{\partial \alpha_f}{\partial \delta_f} = -1, \\ \frac{\partial \alpha_r}{\partial v} &= \frac{\gamma l_r \cos \beta}{v^2 - 2v \gamma l_r \sin \beta + \gamma^2 l_r^2}, \\ \frac{\partial \alpha_r}{\partial \beta} &= \frac{v^2 - \gamma l_r \cos \beta}{v^2 - 2v \gamma l_r \sin \beta + \gamma^2 l_r^2}, \quad \frac{\partial \alpha_r}{\partial \gamma} = \frac{-l_r}{v^2 - 2v \gamma l_r \sin \beta + \gamma^2 l_r^2}. \end{aligned}$$

The vehicle drifting motion is under the unique motion when forces between tires and the ground reach the maximum. According to the drifting motion characteristics, the status parameter values of the narrow tilting vehicle drifting motion can be calculated based on Equations (1)–(4) and play an important role as the target in the narrow tilting vehicle drifting realization. In order to simplify the controller design, considering the target drifting motion, the state-space expression of the narrow tilting dynamics model Equation (12) is derived as follows.

$$\dot{x} = Ax + B_u u, \tag{13}$$

where $x = [v - v_{target} \quad \beta - \beta_{target} \quad \gamma - \gamma_{target}]^T$ is the state vector of system, $u = [\delta_f - \delta_{f_target} \quad \kappa_f - \kappa_{f_target} \quad \kappa_r - \kappa_{r_target}]^T$ is the control input of system, and coefficient matrices A and B_u are derived based on Equation (12) with the current and target motions.

3.2. Robust Controller

Combing Equation (13), the narrow tilting vehicle drifting control system with uncertain extern disturbances can be described as Equation (14).

$$\begin{cases} \dot{x} = Ax + B_u u + B_d d_e \\ y = x \\ z = [C_Q, \mathbf{0}_{3 \times 3}]^T x + [\mathbf{0}_{3 \times 3}, C_R]^T u \end{cases}, \tag{14}$$

where y is the measurement output of system, z is the controlled output pf system, $d_e = [d_\delta \quad d_f \quad d_r]^T$ and $d_\delta, d_f,$ and d_r are uncertain extern disturbances concerned with inputs, the coefficient matrix B_d expresses the correlation between the differential state vector and the disturbance vector, coefficient matrices C_Q and C_R are symmetric matrices and $C_Q > 0$, and the symbol $\mathbf{0}_{3 \times 3}$ expresses the null matrix with three rows and three columns.

The robust state-feedback control law is designed as:

$$u = Kx, \tag{15}$$

where K is the control gain matrix.

The robust cost function is designed as:

$$J = \int_0^t z^T z dt = \int_0^t (x^T Q x + u^T R u) dt, \tag{16}$$

where weight matrices Q and R , respectively, equal $C_Q^T C_Q$ and $C_R^T C_R$.

To ensure the antijamming capability of the narrow tilting vehicle drifting control system, it need be suppressed that the uncertain extern disturbances impact on the controller performance. Thus, the cost function in Equation (16) needs to satisfy the following:

$$\int_0^t (x^T Q x + u^T R u) dt < \rho^2 \int_0^t d_e^T d_e dt, \tag{17}$$

where ρ is the scalar to express the anti-disturbance capability and $\rho > 0$.

To guarantee the convergence of the control system towards the balance state, the Lyapunov stability is satisfied and the Lyapunov function and the derived function are selected as follows:

$$L = x^T P x, \tag{18}$$

$$\dot{L} = \dot{x}^T P x + x^T P \dot{x}, \tag{19}$$

where the matrix P is the positive definite symmetric matrix.

The Lyapunov derived function Equation (19) can be derived as:

$$\dot{L} = \lambda^T \begin{bmatrix} P_s^T + P_s & PB_d \\ B_d^T P & 0_{3 \times 3} \end{bmatrix} \lambda, \tag{20}$$

where the vector λ is the set of the state vector and the uncertain extern disturbance vector and $\lambda = [x^T, d_e^T]^T$, the matrix P_s represents the operation $P(A + B_u K)$, and the matrix $0_{3 \times 3}$ expresses the null matrix with three rows and three columns.

The derived function of the cost function Equation (16) can be described as:

$$x^T Q x + u^T R u - \rho^2 d_e^T d_e = \lambda^T \begin{bmatrix} Q + K^T R K & 0_{3 \times 3} \\ 0_{3 \times 3} & -\rho^2 E_{3 \times 3} \end{bmatrix} \lambda \tag{21}$$

where the symbol $E_{3 \times 3}$ expresses the unit matrix with three rows and three columns.

When combining Equations (20) and (21), the following equation can be obtained:

$$\dot{L} + x^T Q x + u^T R u - \rho^2 d_e^T d_e = \lambda^T \begin{bmatrix} P_s^T + P_s + Q + K^T R K & PB_d \\ B_d^T P & -\rho^2 E_{3 \times 3} \end{bmatrix} \lambda, \tag{22}$$

The result of the control system stability judgment can be obtained based on Equation (22), and the control system will be stable with uncertain external disturbances only if the symmetric matrix in Equation (22) satisfies the following:

$$\begin{bmatrix} P_s^T + P_s + Q + K^T R K & PB_d \\ B_d^T P & -\rho^2 E_{3 \times 3} \end{bmatrix} < 0, \tag{23}$$

Then, Equation (22) can be derived as:

$$\dot{L} + x^T Q x + u^T R u - \rho^2 d_e^T d_e \leq 0, \tag{24}$$

Integrating Equation (24), the cost function satisfies the following:

$$L \leq \rho^2 \int_0^t d_e^T d_e dt - \int_0^t (x^T Q x + u^T R u) dt + L(0) \leq \rho^2 \int_0^t d_e^T d_e dt + L(0) \tag{25}$$

Thus, the following can be derived:

$$P_{min} \|x\|^2 \leq x^T P x \leq \rho^2 \int_0^t d_e^T d_e dt + L(0),$$

$$\|x\|^2 \leq \frac{\rho^2 \int_0^t d_e^T d_e dt + L(0)}{P_{min}}, \tag{26}$$

According to the Schur complement theorem in [29], the following can be derived and Equation (23) can be transformed as Equation (27).

$$\begin{bmatrix} P_s^T + P_s + Q & PB_d & K^T C_R \\ B_d^T P & -\rho^2 E_{3 \times 3} & 0_{3 \times 3} \\ C_R K & 0_{3 \times 3} & -E_{3 \times 3} \end{bmatrix} < 0,$$

$$\begin{bmatrix} P_s^T + P_s & PB_d & K^T C_R & C_Q \\ B_d^T P & -\rho^2 E_{3 \times 3} & 0_{3 \times 3} & 0_{3 \times 3} \\ C_R K & 0_{3 \times 3} & -E_{3 \times 3} & 0_{3 \times 3} \\ C_Q & 0_{3 \times 3} & 0_{3 \times 3} & -E_{3 \times 3} \end{bmatrix} < 0, \tag{27}$$

Because of the equations $P_s = P(A + B_u K)$ and $P_s^T = (A + B_u K)^T P$, Equation (27) becomes the following:

$$\begin{bmatrix} P(A + B_u K) + (A + B_u K)^T P & PB_d & K^T C_R & C_Q \\ B_d^T P & -\rho^2 E_{3 \times 3} & \mathbf{0}_{3 \times 3} & \mathbf{0}_{3 \times 3} \\ C_R K & \mathbf{0}_{3 \times 3} & -E_{3 \times 3} & \mathbf{0}_{3 \times 3} \\ C_Q & \mathbf{0}_{5 \times 3} & \mathbf{0}_{3 \times 3} & -E_{3 \times 3} \end{bmatrix} < 0, \quad (28)$$

To solve the two unknown variable matrices P and K simply, both sides of Equation (28) are multiplied by the matrix $S = \text{diag}\{P^{-1} \ E_{3 \times 3} \ E_{3 \times 3} \ E_{3 \times 3}\}$, and the solution can be calculated by the following LMIs.

$$\begin{bmatrix} P > 0, \\ AP^{-1} + B_u KP^{-1} + P^{-1}A^T + P^{-1}K^T B_u^T & B_d & P^{-1}K^T C_R & P^{-1}C_Q \\ B_d^T & -\rho^2 E_{3 \times 3} & \mathbf{0}_{3 \times 3} & \mathbf{0}_{3 \times 3} \\ C_R KP^{-1} & \mathbf{0}_{3 \times 3} & -E_{3 \times 3} & \mathbf{0}_{3 \times 3} \\ C_Q P^{-1} & \mathbf{0}_{3 \times 3} & \mathbf{0}_{3 \times 3} & -E_{3 \times 3} \end{bmatrix} < 0, \quad (29)$$

The inverse operation and the multiplied operation related to the unknown matrices are expressed as the following for the simplified calculation of Equation (29).

$$R_1 = P^{-1}, \quad (30)$$

$$R_2 = KP^{-1}, \quad (31)$$

Thus, Equation (29) can be derived as Equation (32), and the solution of the equation can be transformed to the solution of Equation (28).

$$\begin{bmatrix} R_1 > 0, \\ AR_1 + B_u R_2 + R_1 A^T + R_2^T B_u^T & B_d & R_2^T C_R & R_1 C_Q \\ B_d^T & -\rho^2 E_{3 \times 3} & \mathbf{0}_{3 \times 3} & \mathbf{0}_{3 \times 3} \\ C_R R_2 & \mathbf{0}_{3 \times 3} & -E_{3 \times 3} & \mathbf{0}_{3 \times 3} \\ C_Q R_1 & \mathbf{0}_{3 \times 3} & \mathbf{0}_{3 \times 3} & -E_{3 \times 3} \end{bmatrix} < 0, \quad (32)$$

According the solution, the control gain matrix K can be calculated and the actual control parameters can be obtained as Equation (33).

$$\begin{bmatrix} \delta_f, \kappa_f, \kappa_r \end{bmatrix}^T = Kx + \begin{bmatrix} \delta_{f_target}, \kappa_{f_target}, \kappa_{r_target} \end{bmatrix}^T, \quad (33)$$

4. Narrow Tilting Vehicle Drifting Control Simulation Results

The narrow tilting vehicle main parameters are shown in Table 1 and the maximum steering angle is 0.52 rad in practice. The satisfying performance of the robust Controller is verified with uncertain disturbances in MATLAB/Simulink. The simulation system is established based on Equations (1)–(4) and Equations (6)–(10), and the uncertain external disturbances are described as random numbers and the coefficient matrix B_d equals the coefficient matrix B_u .

Table 1. The main parameters of the narrow tilting vehicle.

m	m_b	I_z	l_f	l_r	w_r	w_f	h_g
237.1 kg	195.4 kg	243.2 kg·m ²	0.73 m	0.80 m	0.68 m	0.70 m	0.42 m

The narrow tilting vehicle drifting controller is calculated and obtained with the steady-state target drifting motion in Table 2, which can be obtained by the analysis of the

narrow tilting vehicle drifting motion state parameters in the condition that tire forces reach the maximum. Furthermore, the narrow tilting vehicle drifting controller starts to work under different initial motion conditions in Table 3 to verify that the designed controller has good performance in different conditions.

Table 2. Target drifting motion groups.

Target Group	v_{target}	β_{target}	γ_{target}	δ_{f_target}	κ_{f_target}	κ_{r_target}	μ
(1)	3.49 m/s	−0.32 rad	1.95 rad/s	0.1 rad	0	0.64	0.75
(2)	10 m/s	−0.73 rad	0.71 rad/s	−0.35 rad	0	1	0.75

Table 3. Initial motion groups.

Initial Group	v	β	γ	δ_f	κ_f	κ_r	μ
(1)	5 m/s	0 rad	0 rad/s	0 rad	0	0	0.75
(2)	8 m/s	0 rad	0 rad/s	0 rad	0	0	0.75
(3)	10 m/s	0 rad	0 rad/s	0 rad	0	0	0.75
(4)	12.5 m/s	0 rad	0 rad/s	0 rad	0	0	0.75
(5) *	6 m/s	−0.72 rad	1.16 rad/s	−0.34 rad	0	1	0.75

* A drifting motion.

Considering the steering angle and longitudinal slip ratio ranges in practice, their amplitudes and gains are limited in simulation. The designed controller is used to realize target drifting motions in different initial motion conditions. The simulation results are shown in Figures 7–11, including velocities, sideslip angles, yaw rates, steering angles, longitudinal slip ratios, and position modifications, which suggests the designed controller has a good performance. In Figure 7, the target drifting motion is a typical drifting working condition with a large yaw rate, and the initial motion is a uniform linear motion, and the simulation result suggests the designed controller can realize the drifting motion with a small turning radius at a low velocity and a large yaw rate. Figure 7f suggests that there are smaller vertical load transforms of the active rolling than the normal, which means the narrow tilting vehicle is safer than the normal narrow vehicle in the drifting motion. In Figures 8–10, the target drifting motion is another typical drifting working condition with the maximum longitudinal slip ratio of the rear axle wheels, and the initial motions are uniform linear motions with different velocities, and the simulation results suggest that the designed controller can realize the same target drifting motion with different initial velocities. In Figure 11, the initial motion is a steady-state drifting motion different from others, and the simulation result suggests the designed controller can switch implementations for different drifting motions. Because the controller dynamics model is simplified based on the simulation model, there are some distances from the final state values and the target state values in Figures 7–11, but most relative errors inspected are less than 5%, and the maximum relative error is less than 10%. In addition, because of the significant differences between the target and initial motions and the amplitude and gain limitations of the control inputs, the designed controller needs some implementation time and some slight adjustments for the final state values to accomplish the target motions.

The narrow tilting vehicle with the designed robust drifting controller can realize different target drifting motions in different initial states. The designed controller can realize the narrow tilting vehicle drifting motions with uncertain external disturbances and with the consideration of not only the target drifting state parameters, but also the target drifting control parameters. The controller realizes a typical drifting motion with a large yaw rate, and the final trajectory is a circle with a small turning radius at a low velocity. Additionally, the controller also can realize another typical drifting motion with a large longitudinal slip ratio of the rear axle wheels, and the initial states include different uniform linear motions and a drifting motion. The simulation results suggest that the

designed controller makes it easy for the narrow tilting vehicle to realize different drifting motions with uncertain external disturbances.

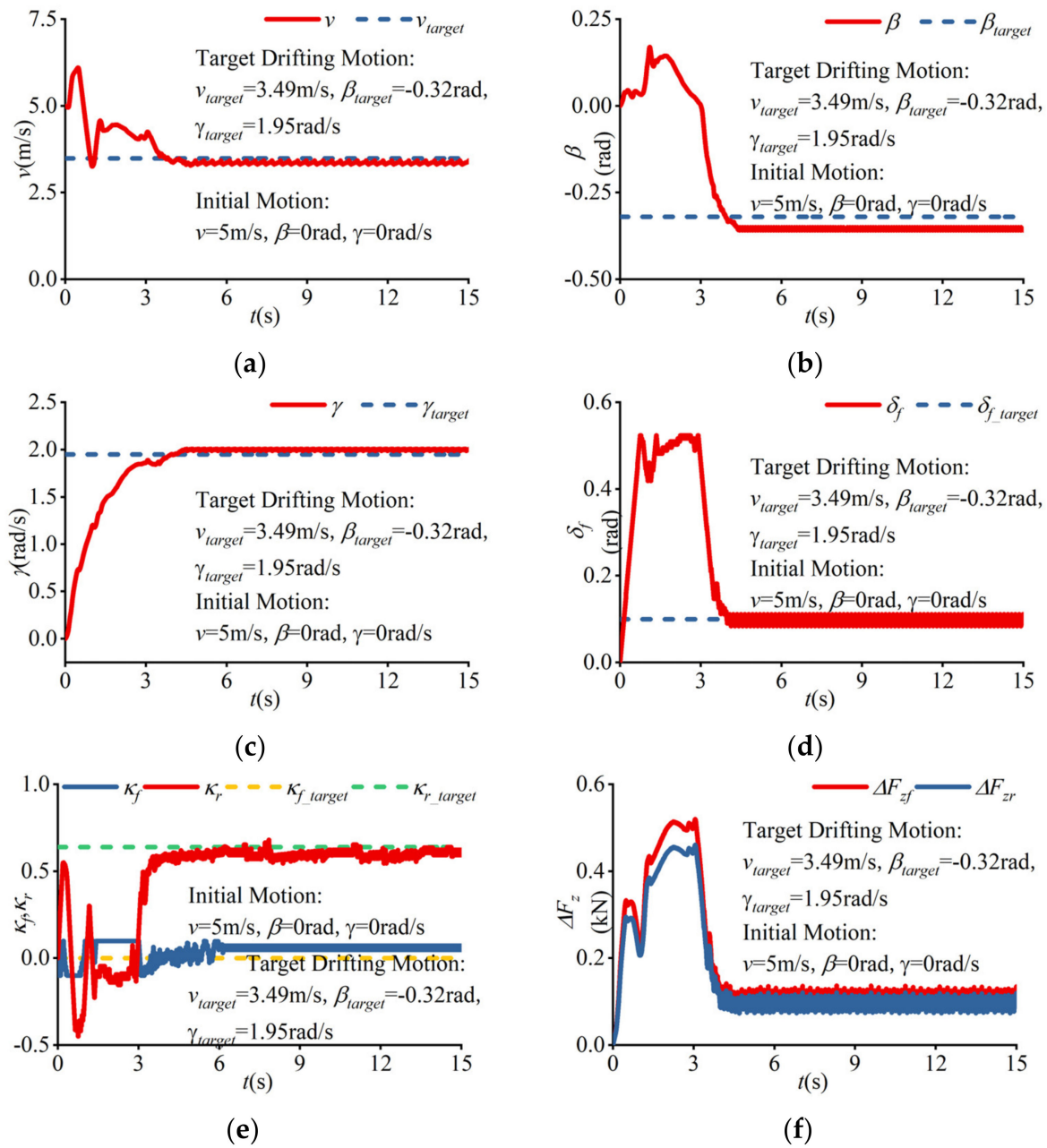


Figure 7. The simulation result with the initial motion as Group 1 in Table 3 to realize the target drifting motion as Group 1 in Table 2: (a) the variation curve of the velocity; (b) the variation curve of the sideslip angle; (c) the variation curve of the yaw rate; (d) the variation curve of the steering angle; (e) the variation curves of the TYDEX longitudinal slip ratios; (f) the differences between the steady-state vertical load transforms of the active rolling and the normal rolling based on Equations (4)–(9), where $\Delta F_{zf} = \left(|F_{zfl} - F_{zfr}|_{\text{normal rolling}} - |F_{zfl} - F_{zfr}|_{\text{active rolling}} \right) / 2$ and $\Delta F_{zr} = \left(|F_{zrl} - F_{zrr}|_{\text{normal rolling}} - |F_{zrl} - F_{zrr}|_{\text{active rolling}} \right) / 2$.

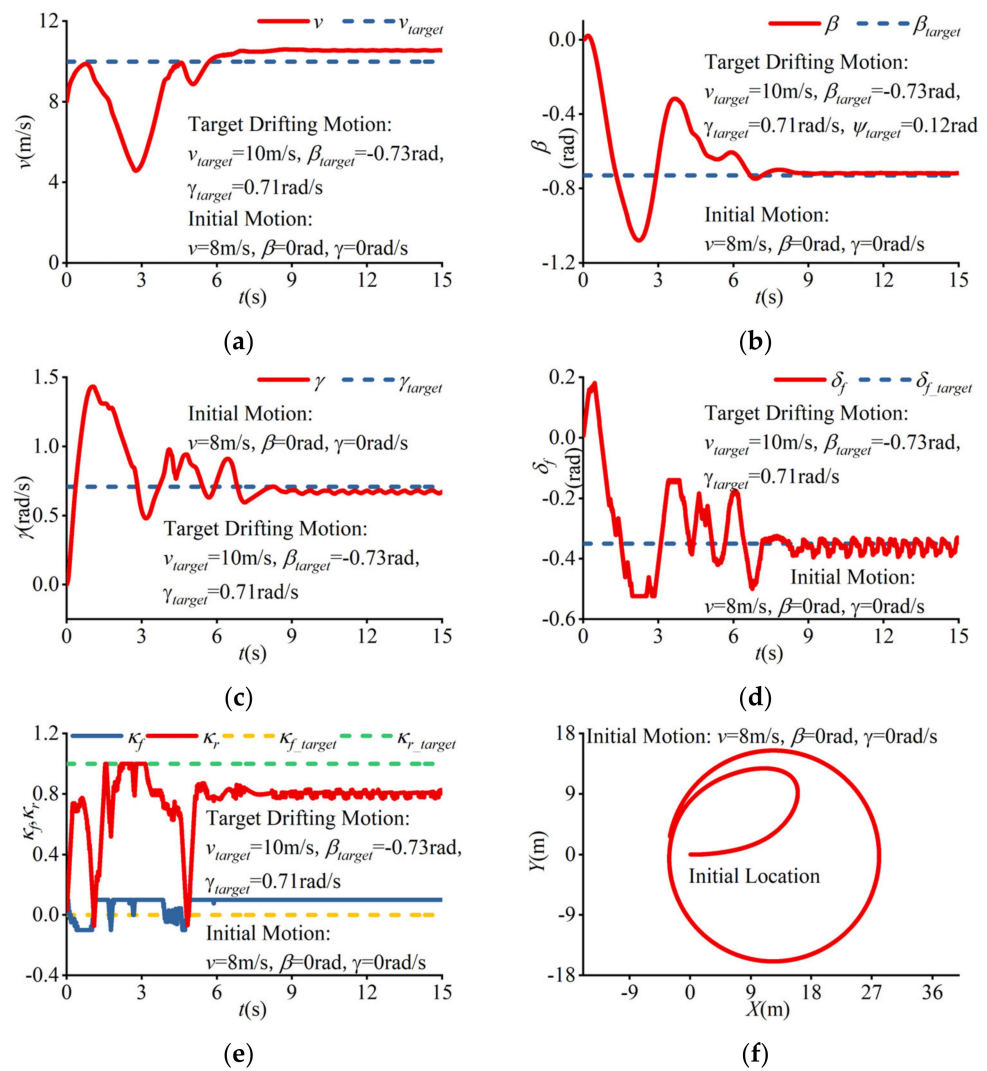


Figure 8. The simulation result with the initial motion as Group 2 in Table 3 to realize the target drifting motion as Group 2 in Table 2: (a) the variation curve of the velocity; (b) the variation curve of the sideslip angle; (c) the variation curve of the yaw rate; (d) the variation curve of the steering angle; (e) the variation curves of the TYDEX longitudinal slip ratios; (f) the position modification of the narrow tilting vehicle in the ground coordinates.

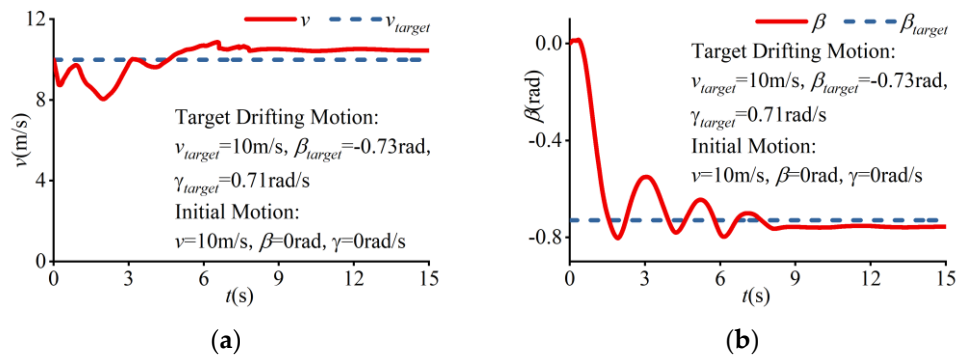


Figure 9. Cont.

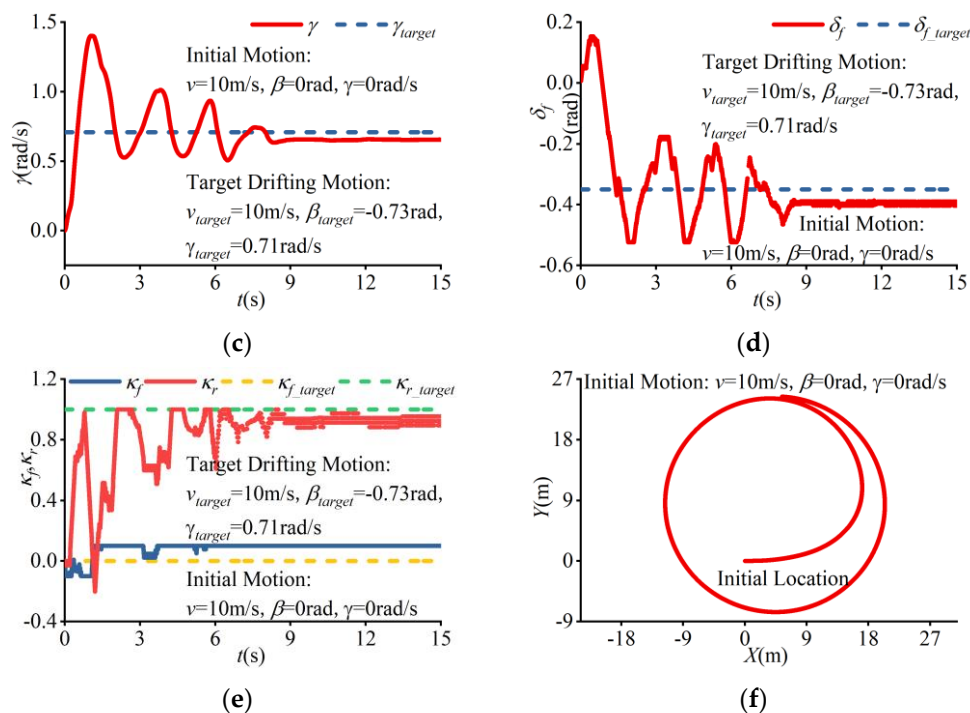


Figure 9. The simulation result with the initial motion as Group 3 in Table 3 to realize the target drifting motion as Group 2 in Table 2: (a) the variation curve of the velocity; (b) the variation curve of the sideslip angle; (c) the variation curve of the yaw rate; (d) the variation curve of the steering angle; (e) the variation curves of the TYDEX longitudinal slip ratios; (f) the position modification of the narrow tilting vehicle in the ground coordinates.

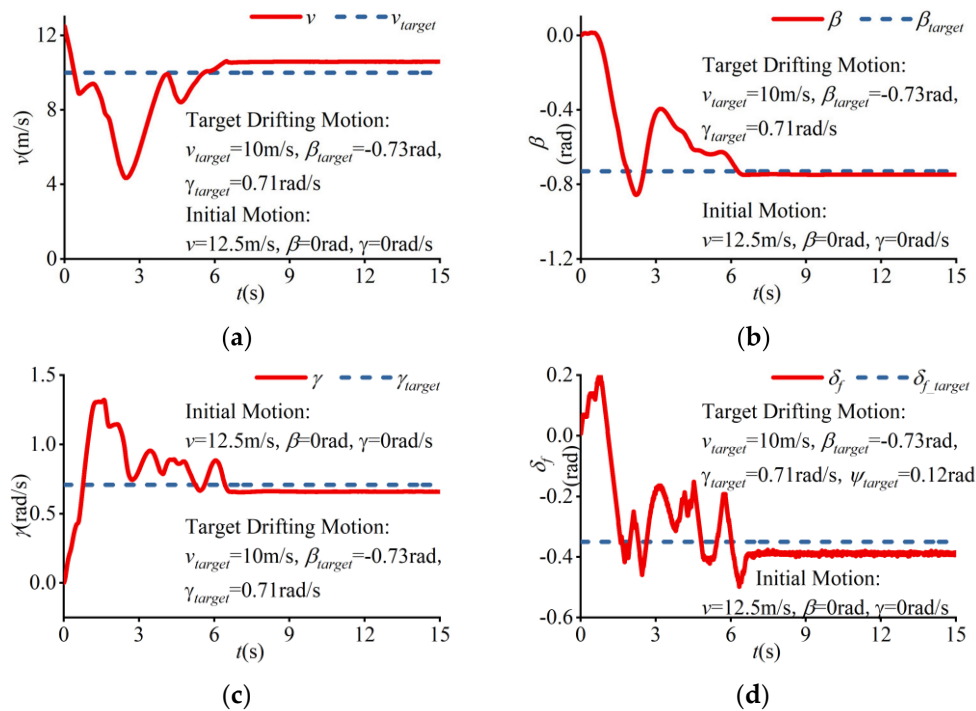


Figure 10. Cont.

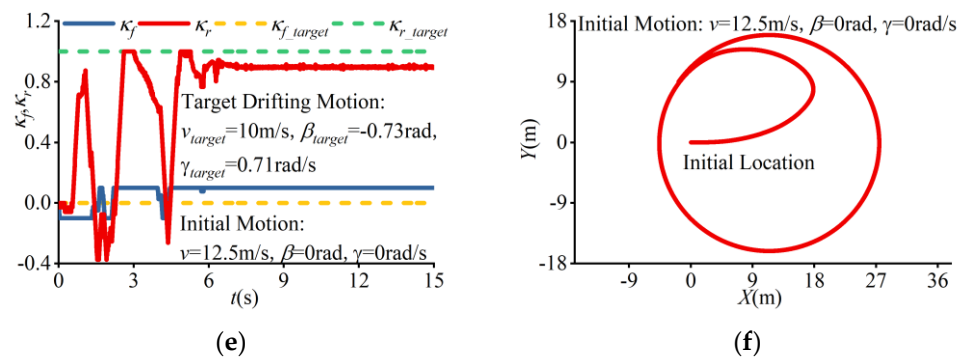


Figure 10. The simulation result with the initial motion as Group 4 in Table 3 to realize the target drifting motion as Group 2 in Table 2: (a) the variation curve of the velocity; (b) the variation curve of the sideslip angle; (c) the variation curve of the yaw rate; (d) the variation curve of the steering angle; (e) the variation curves of the TYDEX longitudinal slip ratios; (f) the position modification of the narrow tilting vehicle in the ground coordinates.

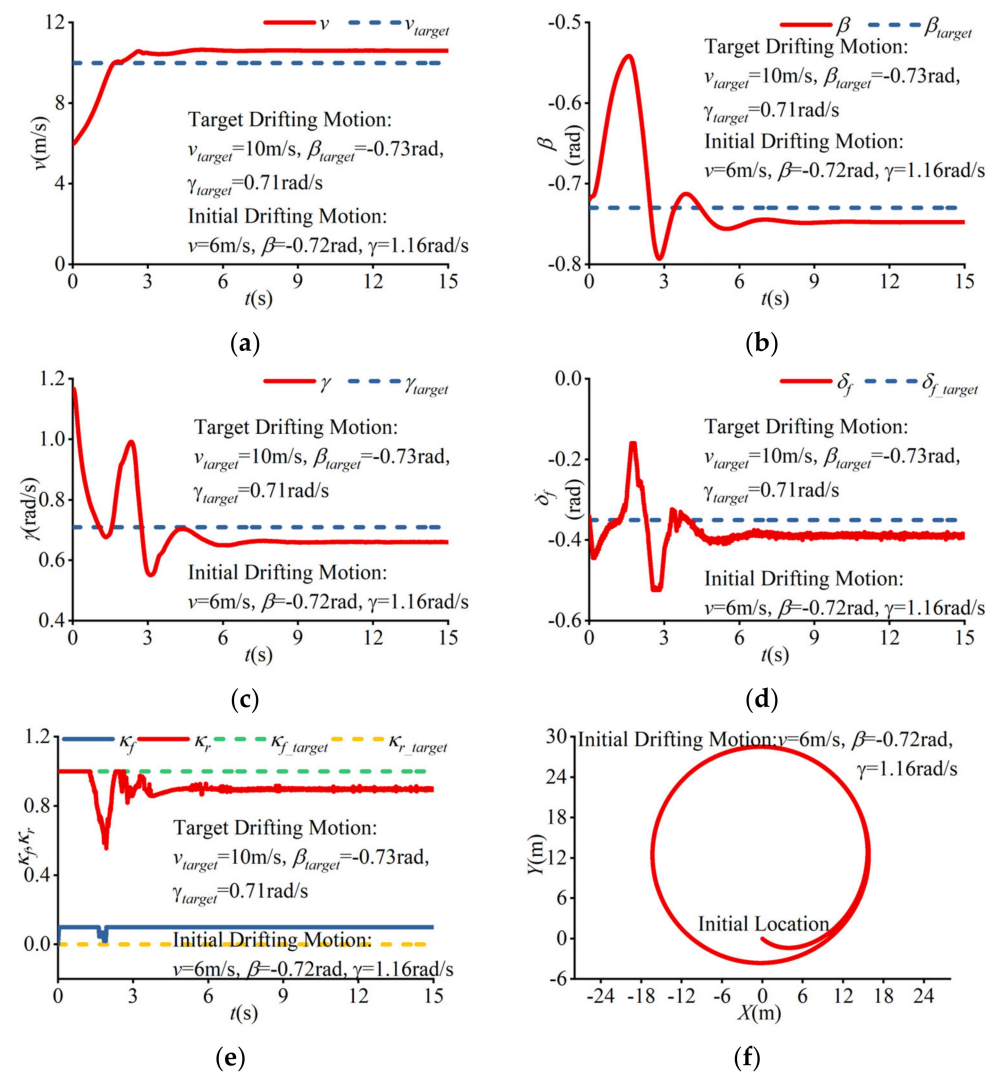


Figure 11. The simulation result with the initial drifting motion as Group 5 in Table 3 to realize the target drifting motion as Group 2 in Table 2: (a) the variation curve of the velocity; (b) the variation curve of the sideslip angle; (c) the variation curve of the yaw rate; (d) the variation curve of the steering angle; (e) the variation curves of the TYDEX longitudinal slip ratios; (f) the position modification of the narrow tilting vehicle in the ground coordinates.

5. Conclusions

This paper researches the drifting motion independent control of the narrow tilting vehicle based on a robust theory with uncertain external disturbances. The drifting control of the narrow tilting vehicle is significant to improve traffic safety based on a narrow tilting vehicle and drifting motion characteristics. According to the active rolling chrematistics, the narrow tilting dynamic model is established to describe the characteristics, and simplified expressions are used in the drifting controller design. With uncertain external disturbances, the drifting controller of the narrow tilting vehicle is designed based on robust theory and calculated by the LMIs to realize narrow tilting vehicle drifting motions and tire limit operations. The controller is tested to realize different drifting motions with different initial motions, which suggests that the controller has a good performance of drifting motion realizations with a wide application. The narrow tilting vehicle drifting control can make the utmost of the vehicle's dynamic performance and improve driving safety, especially when tires reach the maximum, which is worth further research.

Author Contributions: Conceptualization, G.W.; methodology, D.X.; software, D.X.; validation, D.X.; formal analysis, G.W., D.X. and Y.W.; investigation, D.X.; resources, Y.W.; data curation, X.H.; writing—original draft preparation, D.X.; writing—review and editing, G.W., Y.H. and X.H.; visualization, Y.H.; supervision, G.W.; project administration, G.W.; funding acquisition, NSFC. All authors have read and agreed to the published version of the manuscript.

Funding: This research was funded by the National Natural Science Foundation of China, grant number 51775548.

Data Availability Statement: Not applicable.

Acknowledgments: The authors would like to thank to all the students taking part in the experiment from the College of Engineering, China Agricultural University. D.X. and G.W. conceived the motion mechanism analysis and the control algorithm, performed the simulations, and finished the manuscript. Y.H. and X.H. revised the paper. Y.W. provided the research subject. The authors gratefully acknowledge the financial support from the National Natural Science Foundation of China (No. 51775548).

Conflicts of Interest: The authors declare no conflict of interest.

References

1. China Association of Automobile Manufacturers. Available online: <http://en.caam.org.cn/Index/show/catid/57/id/1864.html> (accessed on 15 November 2022).
2. World Health Organization. Available online: <https://www.who.int/news-room/fact-sheets/detail/the-top-10-causes-of-death> (accessed on 9 December 2020).
3. World Health Organization. Available online: <https://www.who.int/publications/i/item/9789241565684> (accessed on 17 June 2018).
4. World Health Organization. Available online: <https://www.who.int/zh/news/item/30-06-2022-new-political-declaration-to-halve-road-traffic-deaths-and-injuries-by-2030-is-a-milestone-achievement> (accessed on 30 June 2022).
5. Wu, J.; Tian, Y.; Walker, P.; Li, Y. Attenuation Reference Model Based Adaptive Speed Control Tactic for Automatic Steering System. *Mech. Syst. Signal Process.* **2021**, *156*, 107631. [[CrossRef](#)]
6. Zhang, Z.; Li, Y.; Yu, Y.; Zhang, Z.; Zheng, L. Study on Local Path Planning and Tracking Algorithm of Intelligent Vehicle in Complex Dynamics Environment. *China J. Highw. Transp.* **2022**, *35*, 372–386. [[CrossRef](#)]
7. Wu, J.; Zhang, J.; Tian, Y.; Li, L. A Novel Adaptive Steering Torque Control Approach for Human-Machine-Cooperation Autonomous Vehicles. *IEEE Trans. Transp. Electr.* **2021**, *7*, 2516–2525. [[CrossRef](#)]
8. Claveau, F.; Chevrel, P.; Mourad, L. Non-Linear Control of a Narrow Tilting Vehicle. In Proceedings of the 2014 IEEE International Conference on Systems, Man, and Cybernetics, San Diego, CA, USA, 5–8 October 2014. [[CrossRef](#)]
9. Mourad, F.; Claveau, F.; Chevrel, P. Design of a Two DOF Gain Scheduled Frequency Shaped LQ Controller for Narrow Tilting Vehicles. In Proceedings of the 2012 American Control Conference, Montreal, Canada, 27–29 June 2012. [[CrossRef](#)]
10. Barker, M.; Drew, B.; Darling, J.; Edge, K.A.; Owen, G.W. Steady-State Steering of a Tilting Three-Wheeled Vehicle. *Veh. Syst. Dyn.* **2010**, *48*, 815–830. [[CrossRef](#)]
11. Rajamani, R.; Gohl, L.; Alexander, L.; Starr, P. Dynamics of Narrow Tilting Vehicles. *Math. Comput. Model. Dyn. Syst.* **2003**, *9*, 209–231. [[CrossRef](#)]
12. Zhang, J. Research on Active Tilt Control Technology for Vehicle Steering. Master's Thesis, China Agricultural University, Beijing, China, 2022.

13. Liu, P.; Ke, C.; Gao, R.; Li, H.; Wei, W.; Wang, Y. Design and Test of Active Roll Vehicle. *Automot. Eng.* **2020**, *42*, 1552–1557, 1584. [[CrossRef](#)]
14. Zhang, J.; Li, H.; Gao, R.; Wang, Y.; Wei, W.; Wang, B. Research and Test on the Stability of Active Rollover Three-wheeled Vehicle. In Proceedings of the 2021 China SAE Congress and Exhibition (SAECCE), Shanghai, China, 19–21 October 2021.
15. Gao, R.; Li, H.; Zhang, J.; Wang, Y.; Wei, W.; Wang, B. Research on Steering Comfort of Active Tilting Vehicles. In Proceedings of the 2021 China SAE Congress and Exhibition (SAECCE), Shanghai, China, 19–21 October 2021.
16. Bianco, A.D.; Roberto, L.; Marco, M. Minimum Time Optimal Control Simulation of a GP2 Race Car. *Inst. Mech. Eng. J. Automob. Eng.* **2018**, *232*, 1180–2232. [[CrossRef](#)]
17. Velenis, E.; Frazzoli, E.; Tsiotras, P. On Steady-State Cornering Equilibria for Wheeled Vehicles with Drift. In Proceedings of the Joint 48th IEEE Conference on Decision and Control and 28th Chinese Control Conference, Shanghai, China, 16–18 December 2009.
18. Zhang, F. Trajectory Planning and Motion Control for Extreme Maneuvers of Autonomous Vehicles. Ph.D. Thesis, Tsinghua University, Beijing, China, 2018.
19. Li, B. Study on Rear Distributed Drive Vehicles Control under Extreme Drifting Maneuvers. Master's Thesis, Jilin University, Changchun, China, 2022.
20. Jelavic, E.; Gonzales, J.; Borrelli, F. Autonomous Drift Parking using a Switched Control Strategy with Onboard Sensors. *Sci. Direct* **2017**, *50*, 2714–3719. [[CrossRef](#)]
21. Qiao, W. Research on the Control Method of Vehicle Drifting Motion under Extreme Conditions. Master's Thesis, Haerbin Institute of Technology, Haerbin, China, 2022.
22. Wang, H.; Zuo, J.; Liu, S.; Zheng, W.; Wang, L. Model-free adaptive control of steady-state drift of unmanned vehicles. *Control. Theory Appl.* **2021**, *38*, 23–32. [[CrossRef](#)]
23. Spielberg, N.A.; Brown, M.; Kapania, N.R.; Kegelman, J.C.; Gerdes, J.C. Neural network vehicle models for high-performance automated driving. *Sci. Robot.* **2019**, *4*, eaaw1975. [[CrossRef](#)] [[PubMed](#)]
24. Pacejka, H.B. *Tyre and Vehicle Model*, 2nd ed.; Elsevier: Oxford, UK, 2006; pp. 16–60.
25. Zuoqiweilai. Available online: <http://www.allinride.com/> (accessed on 5 December 2022).
26. Guo, K.; Lu, D.; Chen, S.; Lin, W.C.; Lu, X. The UniTire model: A nonlinear and non-steady-state tyre model for vehicle dynamics simulation. *Veh. Syst. Dyn.* **2005**, *43*, 341–358. [[CrossRef](#)]
27. Guo, K. UniTire: Unified Tire Model. *J. Mech. Eng.* **2016**, *52*, 90–98. [[CrossRef](#)]
28. Xu, N. Study on the Steady State Tire Model under Combined Conditions. Ph.D. Thesis, Jilin University, Changchun, China, 2012.
29. Wu, J.; Kong, Q.; Yang, K.; Liu, Y.; Cao, D.; Li, Z. Research on the Steering Torque Control for Intelligent Vehicles Co-Driving with the Penalty Factor of Human–Machine Intervention. *IEEE Trans. Syst. Man Cybern. Syst.* **2023**, *53*, 59–70. [[CrossRef](#)]

Disclaimer/Publisher's Note: The statements, opinions and data contained in all publications are solely those of the individual author(s) and contributor(s) and not of MDPI and/or the editor(s). MDPI and/or the editor(s) disclaim responsibility for any injury to people or property resulting from any ideas, methods, instructions or products referred to in the content.